International Journal of Biological Macromolecules 79 (2015) 711–718

Contents lists available at ScienceDirect

International Journal of Biological Macromolecules

journal homepage: www.elsevier.com/locate/ijbiomac

Chameleon 'aggregation-prone' segments of apoA-I: A model of amyloid fibrils formed in apoA-I amyloidosis

Nikolaos N. Louros [a], Paraskevi L. Tsiolaki [a], Michael D.W. Griffin [b], Geoffrey J. Howlett [b], Stavros J. Hamodrakas [a], Vassiliki A. Iconomidou [a,*]

[a] Department of Cell Biology and Biophysics, Faculty of Biology, University of Athens, Panepistimiopolis, Athens 157 01, Greece
[b] Department of Biochemistry and Molecular Biology, Bio21 Molecular Science and Biotechnology Institute, The University of Melbourne, Parkville, VIC 3010, Australia

ARTICLE INFO

Article history:
Received 3 February 2015
Received in revised form 20 May 2015
Accepted 22 May 2015
Available online 3 June 2015

Keywords:
Familial apolipoprotein A-I amyloidosis
"Aggregation-prone" peptide-analogues
Amyloid fibrils

ABSTRACT

Apolipoprotein A-I (apoA-I) is the major component of high density lipoproteins and plays a vital role in reverse cholesterol transport. Lipid-free apoA-I is the main constituent of amyloid deposits found in atherosclerotic plaques, an acquired type of amyloidosis, whereas its N-terminal fragments have been associated with a hereditary form, known as familial apoA-I amyloidosis. Here, we identified and verified four "aggregation-prone" segments of apoA-I with amyloidogenic properties, utilizing electron microscopy, X-ray fiber diffraction, ATR FT-IR spectroscopy and polarized light microscopy. These segments may act as conformational switches, possibly controlling the transition of the α-helical apoA-I content into the "cross-β" architecture of amyloid fibrils. A structural model illuminating the structure of amyloid fibrils formed by the N-terminal fragments of apoA-I is proposed, indicating that two of the identified chameleon segments may play a vital part in the formation of amyloid fibrils in familial apoA-I amyloidosis.

1. Introduction

Human mature apolipoprotein A-I (apoA-I) is a 243 amino acid long protein expressed mainly in the liver and the small intestine [1]. It is encoded by exons 3 and 4 of the homonym gene located at chromosome 11, in the form of a 267-residue pre-pro-protein [2]. Following cleavage of the signal peptide, it is secreted as pro-apoA-I into plasma where it is finally cleaved into its mature form [3]. The apoA-I^{1-43} N-terminal portion is expressed by exon 3 and contains three 11-mer repetitive segments, named G1, G2 and G3, following the first 10 sequence residues [4]. The apoA-I^{44-261} part is expressed by exon 4 and is composed of 10 tandem 11/22-mer repeats which lead to the formation of amphipathic α-helices [5,6]. ApoA-I is the major protein constituent of high density lipoproteins (HDL), contributing in reverse cholesterol transport by promoting efflux of cholesterol and phospholipid from peripheral tissues [7]. Moreover, it serves as an activator of the enzyme lecithin:cholesterol acyltransferase (LCAT) [8]. However, a small percentage of lipid-free apoA-I is also found in plasma with suggested cardioprotective abilities [9].

Apart of its functional properties, apoA-I has been associated with a hereditary and a non-hereditary or acquired type of amyloidosis. Several autosomal dominant mutations, most of them occurring within the first 100 residues of the N-terminal part of apoA-I have been associated with the former type, known as familial apoA-I amyloidosis [10]. Most of the known mutations seem to favor the proteolytic cleavage of apoA-I at a region spanning residues 83–100, after a putative β-breaking motif (EKETEG) encompassing residues 76–81 (Fig. 1) [11]. The resulting, variable in size, N-terminal fragments are co-deposited within amyloid deposits found in various organs and tissues causing neuropathies, nephropathies, hepatopathies and cardiomyopathies [12]. Additionally, *in vitro* studies have also indicated the ability of apoA-I^{1-93}, which is the main constituent of apoA-I fibrillar deposits located in the heart [12], to form amyloid fibrils at acidic conditions [13]. However, wild-type apoA-I is also associated with a non-hereditary type of amyloidosis, since it produces amyloid deposits, commonly located within atherosclerotic plaques [14]. Notably, oxidative conditions induce full length apoA-I aggregation thus further promoting atherogenesis [15].

Abbreviations: ApoA-I, apolipoprotein A-I; ApoC-II, apolipoprotein C-II; HDL, high density lipoprotein; LCAT, lecithin:cholesterol acyltransferase; ATR FT-IR spectroscopy, attenuated total reflectance Fourier-transform spectroscopy.

* Corresponding author. Tel.: +30 210 7274871; fax: +30 210 7274254.
E-mail address: veconom@biol.uoa.gr (V.A. Iconomidou).

http://dx.doi.org/10.1016/j.ijbiomac.2015.05.032
0141-8130/

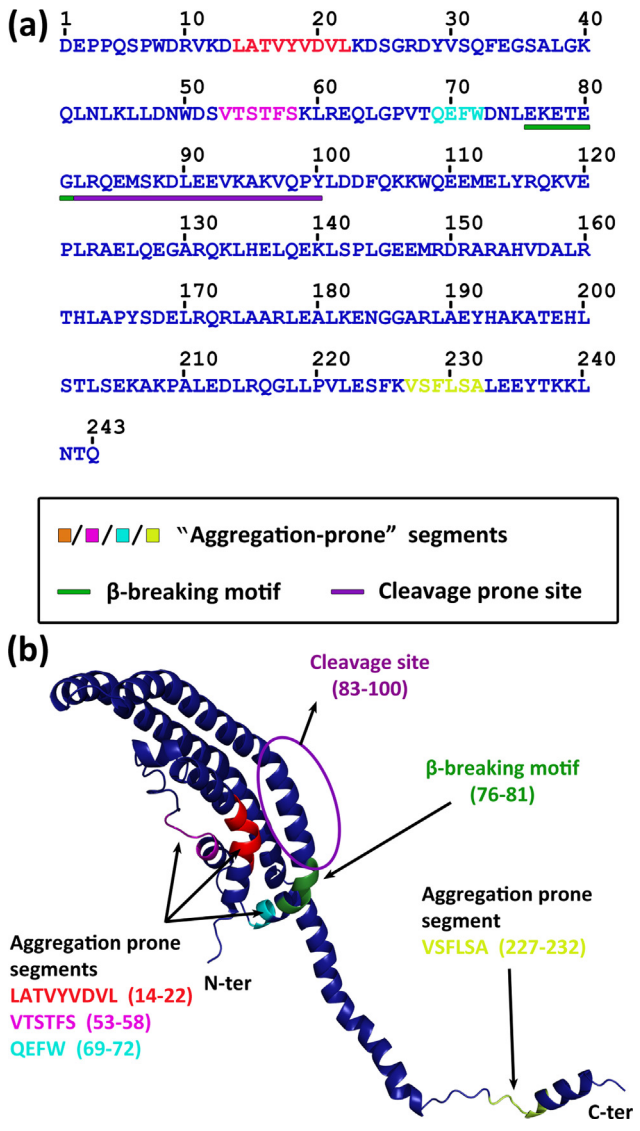

Fig. 1. Prediction of amyloidogenic regions within the apoA-I sequence. (a) The primary structure of human apoA-I. Three "aggregation-prone" regions are located close to the N-terminal part of the protein, ^{14}LATVYVDVL^{22} (shown in red), ^{53}VTSTFS^{58} (shown in magenta) and ^{69}QEFW^{72} (shown in cyan), whereas a fourth segment ^{227}VSFLSA^{232} (shown in lemon) is located close to the C-terminal. (b) Representation of the pseudo full length lipid free apoA-I structure, derived by modeling techniques combining the crystal structures Δ(185–243)apoA-I (residues 1–184) (PDB ID: 3R2P) [46] and Δ(1–43)apoA-I (residues 185–243) (PDB ID: 1AV1) [47], as proposed by Mei and Atkinson [46]. The two individual protein domains are oriented relatively arbitrary and do not depict the actual conformation of the full length protein, since recent MD simulations indicate that the C-terminal domain adopts a dynamic conformation and is loosely wrapped around the N-terminal four helix bundle [48]. Location of all four predicted "aggregation-prone" regions is shown, in addition to the proposed β-breaking motif and the cleavage prone site of the apoA-I N-terminal domain [24]. (For interpretation of the references to color in this figure legend, the reader is referred to the web version of this article.)

Extensive experimental data have consistently indicated that amyloid fibril formation is initiated by short sequence regions, which possess significant self-aggregation propensity and as a result mediate the aggregation tendency of a protein [16–21]. Detailed studies have been performed in order to locate similar "aggregation-prone" segments within the apoA-I sequence. Synthetic N-terminal fragments, such as apoA-I$^{9–28}$, apoA-I$^{1–43}$, apoA-I$^{46–59}$, apoA-I$^{44–65}$ and apoA-I$^{66–83}$ have been shown to lead to the formation of amyloid fibrils in various *in vitro* conditions [22–24]. Moreover, recent impressive work has shown that hydrophobic clusters comprising residues 9–24, 45–63 and the C-terminal segment 221–239 of apoA-I form amyloid fibrils *in vitro* [25]. Finally, recent computational analysis by Gursky and coworkers, utilizing PASTA [26] and two consensus algorithms AMYLPRED and AMYLPRED2 [27,28], developed by our lab, successfully identified four short "aggregation-prone" peptide segments, ^{14}LATVYVDVL^{22}, ^{53}VTSTFS^{58}, ^{69}QEFW^{72} and ^{227}VSFLSA^{232} that may act as amyloidogenic "hot spots", facilitating N-terminal and full length apoA-I polymerization in familial and acquired apoA-I amyloidosis, respectively [24]. In this study, we attempt to verify this assumption experimentally by applying transmission electron microscopy, Congo red staining and polarizing microscopy, X-ray fiber diffraction and ATR FT-IR Spectroscopy studies. Our results clearly indicate that these short stretches act as the core aggregation elements of apoA-I, which may potentially lead in the formation of amyloid fibrils both in familial and acquired apoA-I amyloidosis. Finally, a detailed three-dimensional model of the structure of amyloid fibrils formed by the amyloidogenic N-terminal fragments of apoA-I is proposed indicating that two of the aforementioned "aggregation-prone" peptides, ^{14}LATVYVDVL^{22} and ^{53}VTSTFS^{58} may vitally contribute in the formation of amyloid fibrils associated with familial apoA-I amyloidosis.

2. Materials and methods

2.1. Peptide synthesis and sample preparation

Two consensus tools for the prediction of sequence aggregation propensity, AMYLPRED and AMYLPRED2 [27,28], were applied on the apoA-I sequence. Consequently, three "aggregation-prone" segments, ^{14}LATVYVDVL^{22}, ^{53}VTSTFS^{58} and ^{69}QEFW^{72}, close to the N-terminal of the protein were predicted, in addition to the segment ^{227}VSFLSA^{232} which resides close to the C-terminal, respectively (see Fig. 1). As a result, three peptide analogues, resembling the aforementioned segments ^{14}LATVYVDVL^{22}, ^{53}VTSTFS^{58} and ^{227}VSFLSA^{232} were chemically synthesized. A fourth peptide was also synthesized, containing the "aggregation-prone" ^{69}QEFW^{72} segment, in addition to the preceding V67 and T68 residues in the N-terminus (^{67}VTQEFW^{72}). This decision was based on the fact that both residues display a weaker prediction of aggregation propensity and are also strong β-formers; therefore they may vitally contribute in the formation of a "cross-β" structure. Peptide synthesis was carried out by GeneCust Europe, Luxembourg (purity >98%, free N- and C-terminals). Peptide solutions of all lyophilized peptides were prepared in distilled water (pH 5.75) at a concentration of 10 mg/ml. After incubation for a period of 14 days at ambient temperature, all samples produced gels containing mature amyloid-like fibrils, as judged by negative staining studies (see below).

2.2. Transmission electron microscopy (negative staining)

Drops (~5 μl) of fibril containing solutions of the "aggregation-prone" peptides were applied to 400-mesh glow-discharged and carbon-coated copper grids for 60–80 s. The grids were stained with a drop of 2% (w/v) aqueous uranyl acetate for 60 s. Excess stain was removed by blotting with a filter paper. The grids were initially air-dried and examined with a Morgagni^{TM} 268 transmission electron microscope, operated at 80 kV. Digital acquisitions were performed with an 11 Mpixel side-mounted Morada CCD camera (Soft Imaging System, Muenster, Germany).

2.3. Congo red staining and polarized light microscopy

Films containing amyloid fibrils were formed by applying drops of each peptide solution to glass slides and subsequently air-dried

at ambient temperature and humidity. The films were then stained with a 1% Congo red solution in distilled water (pH 5.75) for 20 min, following the typical Romhanyi protocol [29]. Excess stain was removed through tap water washes [29]. All samples were observed under bright field illumination and between crossed polars, using a Leica MZ75 polarizing stereomicroscope equipped with a JVC GC-X3E camera.

2.4. X-ray fiber diffraction

Droplets (10 μl) of the fibril containing solutions were placed between two aligned capillaries with wax-covered ends (spaced 2 mm apart). The droplets were allowed to dry slowly at ambient temperature and humidity, for 30–60 min in order to form oriented fibers suitable for X-ray diffraction. X-ray diffraction patterns were collected, using a SuperNova-Agilent Technologies X-ray generator equipped with a 135-mm ATLAS CCD detector and a 4-circle kappa goniometer, at the Institute of Biology, Medicinal Chemistry and Biotechnology, National Hellenic Research Foundation (CuK_α high intensity X-ray micro-focus source, $\lambda = 1.5418$ Å), operated at 50 kV, 0.8 mA. The specimen-to-film distance was set at 52 mm. Exposure times were set to 240, 200, 220 and 200 s for peptides ^{14}LATVYVDVL^{22}, ^{53}VTSTFS^{58}, ^{67}VTQEFW^{72} and ^{227}VSFLSA^{232}, respectively. The X-ray patterns, initially viewed using the program CrysAlisPro [30] were displayed and measured with the aid of the program iMosFLM [31].

2.5. Attenuated total reflectance Fourier-transform infrared spectroscopy and post-run spectra computations

Drops (5 μl) of the fibril suspensions were cast on flat stainless-steel plates, coated with an ultrathin hydrophobic layer (SpectRIM, Tienta Sciences, Inc. Indianapolis, USA) and were left to air-dry slowly at ambient conditions, to form thin hydrated films. IR spectra were obtained at a resolution of 4 cm^{-1}, utilizing an IR microscope (IRScope II, BrukerOPTICS, Bruker Optik GmbH, Ettlingen, Germany), equipped with a Ge ATR objective lens (20×) and attached to a FT spectrometer (Equinox 55, BrukerOPTICS). Ten 32-scan spectra were collected from each sample and averaged to improve the sound/noise (S/N) ratio. All spectra are shown in the absorption mode after correction for the wavelength-dependence of the penetration depth (d_p analogous to λ). Absorption band maxima were determined from the minima in the second derivative of the corresponding spectra. Derivatives were computed analytically using routines of the Bruker OPUS/OS2 software, including smoothing over a ±8 cm^{-1} range around each data point, performed by the Savitsky–Golay algorithm [32]. Smoothing over narrower ranges resulted in deterioration of the S/N ratio and did not increase the number of minima that could be determined with confidence. The minima in the second derivative were used to determine the corresponding absorption band maxima.

2.6. Modeling of apoA-I amyloid fibrils

A detailed solenoid-like structure has been previously proposed to depict the structure of amyloid fibrils formed by apolipoprotein C-II (apoC-II). This β-strand–loop–β-strand structure, derived through multiple structural and biophysical methods and using MD simulations, suggests that parallel in-register β-sheets are formed along the axis of the fibril which is formulated by progressively stacked monomers [33]. Luo et al. [34] suggested that the G1, G2 and G3 11-mer repeats of apolipoproteins have been derived through triplication of an initial 11-mer segment. Therefore, it is obvious that all the G-block repeats of apolipoproteins exhibit an apparent sequence homology. Additionally, it has been suggested that the 22-mer repeats of apoA-I have derived through successive

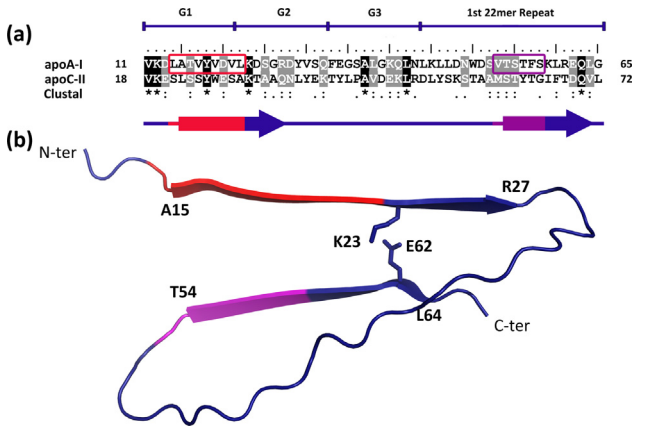

Fig. 2. (a) Sequence alignment of the apoA-I$^{11–65}$ fragment containing the N-terminal 11-mer G1, G2, G3 repeats and the succeeding first 22-mer repeat of apoA-I with the relative G1, G2, G3 repeats and C-terminal remnant of apoC-II. The "aggregation-prone" peptides ^{14}LATVYVDVL^{22} and ^{53}VTSTFS^{58} are labeled with red and purple boxes, respectively. (b) Structural representation of the apoA-I$^{11–65}$ modeled monomer. Residues K23 and E62 which are shown in sticks participate in the formation of intermolecular salt bonds between successive monomers. The "aggregation-prone" ^{14}LATVYVDVL^{22} and ^{53}VTSTFS^{58} peptides correspond to major parts of the facing β-strands extending between residues A15–R27 and T54–L64 of the monomer (shown in red and magenta, respectively). (For interpretation of the references to color in this figure legend, the reader is referred to the web version of this article.)

evolutionary duplication events of the primary 11 residue long C-terminal part of apoC-I which was initially duplicated forming the 22 residue long C-terminal fragment in apoC-II [35]. Based on the above, apoC-II$^{18–72}$ evidently exhibits a high sequence homology with the G1, G2, G3 and first 22-mer repeat of apoA-I (Fig. 2a), a region encompassing residues 11–65 of apoA-I. The amino acid sequence of human apoA-I and apoC-II were extracted from Uniprot (Accession Nos. P02647 and P02655, respectively) [36]. Sequence alignment was performed for the sequence segments 11–65 and 18–72 of apoA-I and apoC-II, respectively, containing the proposed G1, G2 and G3 11-mer repeats along with the first 22-mer repetitive unit of both proteins (Fig. 2a) [35] using ClustalW [37]. Sequence threaded modeling was carried out utilizing Modeller9v12 [38], based on the aforementioned alignment and by using the proposed model structure of apoC-II as a template. As a result, a three-dimensional structure of the 11–65 region of apoA-I was constructed (Fig. 2b) (coordinates are available upon request). The derived model was minimized utilizing the MMTK toolkit [39], which is included in the Chimera molecular graphics system [40] and further evaluated using DSSP and the WHATIF package [41].

3. Results

All three N-terminal (^{14}LATVYVDVL^{22}, ^{53}VTSTFS^{58}, ^{67}VTQEFW^{72}) and the C-terminal (^{227}VSFLSA^{232}) peptide-analogues were found to self-assemble into mature amyloid-like fibrils, after an incubation period of 2 weeks. The fibrils were judged to be mature observing the samples for shorter and longer periods than 2 weeks. Amyloid-like fibrils derived by self-aggregation of peptides ^{14}LATVYVDVL^{22} and ^{67}VTQEFW^{72} appear as straight and unbranched uniform fibrils with an indeterminate length, presenting a small difference in width, since ^{14}LATVYVDVL^{22} fibrils have a larger diameter of approximately 100–120 Å (Fig. 3a), whereas ^{67}VTQEFW^{72} are about 70–90 Å in diameter (Fig. 3c), respectively. Comparably, self-polymerization of the ^{53}VTSTFS^{58} peptide and the C-terminal ^{227}VSFLSA^{232} peptide leads to the formation of protofibrils, which also appear straight and

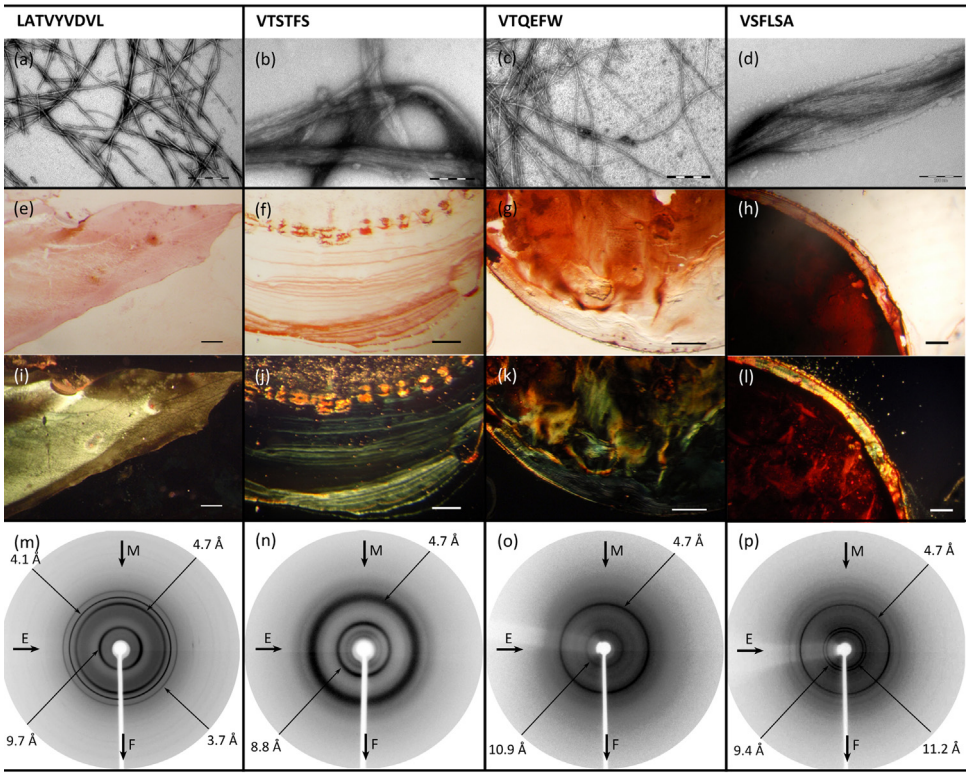

Fig. 3. Amyloidogenic properties of the ^{14}LATVYVDVL^{22}, ^{53}VTSTFS^{58} ^{67}VTQEFW^{72} and ^{227}VSFLSA^{232} "aggregation-prone" peptides. (a–d) The peptide-analogues self-assemble forming straight and unbranched amyloid-like fibrils with an indeterminate length (Scale bars 200 nm). (e–h) Fibril-containing gels bind the Congo red dye as seen under bright field illumination (Scale bars 400 μm). (i–l) An apparent apple/green birefrigence, characteristic for amyloid deposits, is clearly seen under crossed polars (Scale bars 400 μm). (m–p) X-ray fiber diffraction patterns exhibit the typical to a "cross-β"-like architecture reflections, with a 4.7 Å repeat corresponding to the distance of hydrogen bonded β-strands aligned perpendicularly to the fiber axis and the 9.7, 8.8, 10.9 and 11.2 Å reflections representing the distance between the packed β-sheets that are aligned parallel to the same axis. (For interpretation of the references to color in this figure legend, the reader is referred to the web version of this article.)

unconnected, but they have smaller diameters, approximately 30–50 Å. Furthermore, they present a high tendency to coalesce in a latteral fashion, forming thick and variable in size ribbons of protofibrils (Fig. 3b, d).

Gels containing amyloid-like fibrils, derived by self-aggregation of all four peptide-analogues, were stained with the Congo red dye. Congo red has been shown to specifically bind on amyloid fibrils and produce a characteristic yellow/green birefringence, when viewed under crossed polars in a polarizing microscope. In all cases, deposits of amyloid-like fibrils of the peptide-analogues bind the Congo red dye, as seen under bright field illumination (Fig. 3e–h). Furthermore, the typical for amyloid yellow/green birefringence is evident when viewed under crossed polars (Fig. 3i–l).

X-ray diffraction experiments were performed on fibers containing amyloid-like fibrils, derived by self-assembly of each peptide-analogue. The X-ray patterns derived by fibers from each peptide indicate that amyloid fibrils formed by the peptide-analogues possess the typical "cross-β"-like architecture of amyloid fibrils. A strong reflection is present in all cases, corresponding to a 4.7 Å structural repetition, attributed to the interstrand distance between successive hydrogen bonded β-strands that are aligned perpendicular to the fibril axis (Fig. 3m–p). The relatively strong reflections, located at 9.7, 8.8, 10.9 and 11.2 Å, for peptides ^{14}LATVYVDVL^{22}, ^{53}VTSTFS^{58}, ^{67}VTQEFW^{72} and ^{227}VSFLSA^{232}, respectively, are attributed to the varying packing distance between consecutive β-sheets that are aligned parallel to the fiber axis (Fig. 3m–p). This observed variation is possibly explained by the fact that different side chains intervene between the packed β-sheets, in each case. The additional observed 3.7 and 4.1 Å reflections in the ^{14}LATVYVDVL^{22} pattern (Fig. 3m) may be attributed to the wax head of the capillary (Fig. S1) used to obtain an aligned fiber (see Section 2), whereas the 9.4 Å reflection observed in the ^{227}VSFLSA^{232} pattern is most probably a second order of the 4.7 Å reflection. Reflections appear as rings due to poor alignment of the oriented fiber constituent fibrils.

Evidence supporting the X-ray fiber diffraction results were derived by ATR FT-IR spectroscopy studies. ATR FT-IR spectra indicate a predominant β-sheet secondary structure for amyloid fibrils derived by the "aggregation-prone" peptide analogues (Fig. 4a–d). Specifically, a dominant amide I β-sheet band at 1626, 1630, 1631 and 1626 cm^{-1} is seen for ^{14}LATVYVDVL^{22}, ^{53}VTSTFS^{58}, ^{67}VTQEFW^{72} and ^{227}VSFLSA^{232} peptides, respectively (Fig. 4). Additionally, a strong shoulder located at 1693, 1696, 1697 and 1696 cm^{-1}, respectively, may suggest that the β-sheets are in fact antiparallel (Table 1). The ATR FT-IR data regarding the ^{14}LATVYVDVL^{22} and ^{53}VTSTFS^{58} peptides are strongly correlated to the FT-IR data derived by studies of the 1–43 (containing the ^{14}LATVYVDVL^{22} peptide) and 44–65 (containing the ^{53}VTSTFS^{58} peptide) segments, recently reported by Adachi and coworkers [23]. However, FT-IR data derived from the same study indicated that the 66–83 segment of WT apoA-I (containing the ^{67}VTQEFW^{72} peptide) does not lead to the formation of amyloid fibrils but instead retains an α-helical conformation [23].

4. Discussion

The experimental results presented in this work clearly indicate that the four segments of apoA-I identified by our algorithms AMYLPRED and AMYLPRED2, have an intrinsic high aggregation

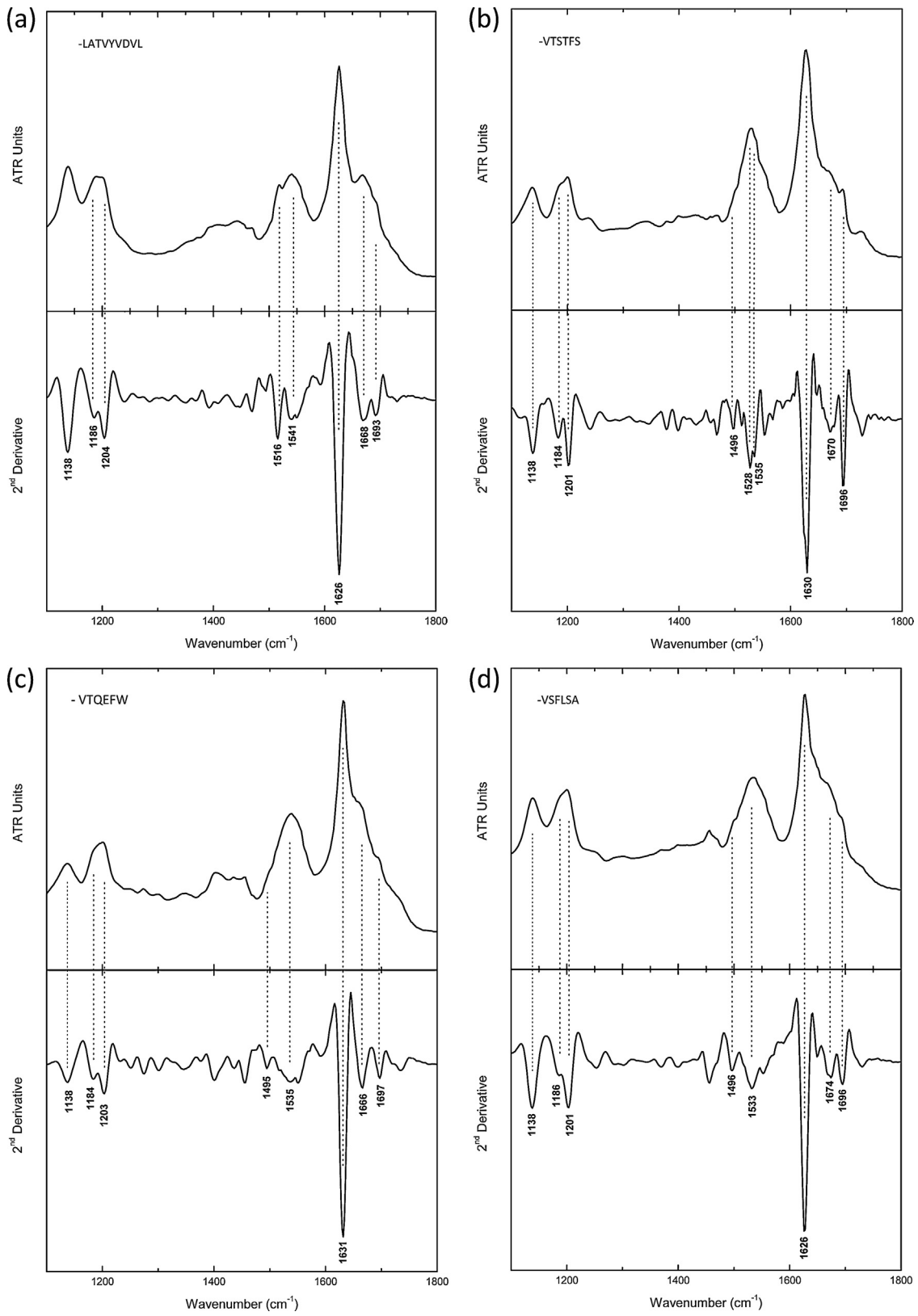

Fig. 4. ATR FT-IR (1100–1800 cm^{-1}) spectra obtained from thin hydrated-films containing amyloid-like fibrils. The thin hydrated-films, formed from fibril solutions of the peptides (a) ^{14}LATVYVDVL^{22}, (b) ^{53}VTSTFS^{58}, (c) ^{67}VTQEFW^{72} and (d) ^{227}VSFLSA^{232}, respectively, were cast on flat stainless-steel plates coated with an ultra thin hydrophobic layer (see Section 2). Second derivative spectra are included and were used for the exact identification of the band maxima and their tentative assignments. All resulting spectra are indicative of the preponderance of an antiparallel β-sheet secondary structure (Table 1).

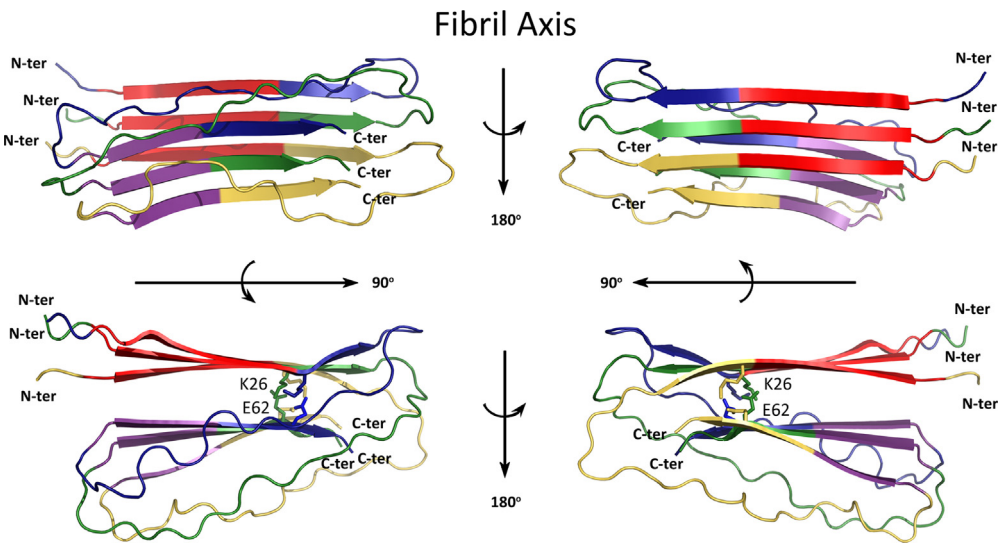

Fig. 5. A hypothetical mechanism of apoA-I amyloid fibril formation in familial apoA-I amyloidosis by the core 11–65 segment containing the "aggregation-prone" ^{14}LATVYVDVL^{22} and ^{53}VTSTFS^{58} peptides. Structural representation of the proposed model (for clarity, three successive monomers are shown in blue, green and yellow, respectively). apoA-I$^{11–65}$ monomers stack along the fibril axis forming two facing β-sheets. Salt bonds formed between residues K23 of each monomer and E62 of the successive monomer further stabilize the overall structure. The "aggregation-prone" peptides ^{14}LATVYVDVL^{22} (shown in red) and ^{53}VTSTFS^{58} (shown in magenta) constitute the major part of the first and second β-strand of each monomer, respectively. Model co-ordinates are available upon request.

tendency, since they lead to the formation of fibrils presenting all basic characteristics of amyloid fibrils.

A possible polymerization model for the apoA-I$^{1–93}$ N-terminal fragment and the full length protein was recently proposed [24]. This analysis was based on previous experimental data indicating that the three N-terminal "aggregation-prone" segments are somewhat protected within the lipid-free structure of apoA-I from self-polymerizing, due to interactions that stabilize the four-α-helix bundle fold [42]. Additionally, the ^{227}VSFLSA^{232} peptide is protected from polymerization, since it is located at the C-terminal end of the protein which is usually bound to lipids. However, when fragmented or found under acidic conditions, these amyloidogenic sequences are allowed to self-assemble leading either apoA-I$^{1–93}$ or the native protein to the formation of amyloid fibrils. Our results support this assumption by indicating that all four peptide-analogues have the tendency to self-polymerize forming amyloid-like filaments.

Computational analysis of the secondary structure of apoA-I was performed utilizing the consensus algorithm SecStr [43] combining six individual secondary structure prediction methods, developed at our lab and NetCSSP which calculates contact-dependent secondary structure propensity [44]. Results indicate that the apoA-I sequence has an eminent propensity to form α-helices, however it also exhibits a smaller propensity to form interrupted β-strands along its full length (Figs. S2 and S3). Furthermore, as indicated by both algorithms, all four "aggregation-prone" stretches have a relatively strong β-structure prediction, implying that they may act as conformational switches. Corroborative evidence suggests that the N- and C-terminal ends of the protein have a higher propensity for a disordered conformation, especially when found within hydrophilic media and/or in the absence of lipid surfaces [25]. These disorder-prone flanking ends were proposed to have a higher propensity to develop a transition from an α-helical to an ordered β-structure, which is facilitated by the presence of specific hydrophobic sequence stretches. The N-terminal ^{14}LATVYV^{19} and ^{52}SVTSTFS^{58} and the C-terminal ^{227}VSFLSAL^{233} segments were proposed as core elements of the flanking hydrophobic stretches, encompassing more or less three of the sequence segments of our study. These regions were proposed to lead to the formation of steric zippers, a notion that is supported by our results indicating that these chameleon segments self-assemble forming amyloid-like fibrils.

A three-dimensional model of the region encompassing residues 11–65 of apoA-I was derived utilizing the previously described model of apoC-II fibrils as template, assuming that the two proteins form similar fibrillar arrangements. The topology of the individual apoC-II monomers comprise a β-strand–loop–β-strand structure, with each monomer contributing two β-strands, one to each β-sheet of the fibril. The model derived by threading the apoA-I sequence onto that of apoC-II suggests that a significant part (11–65) of the amyloidogenic apoA-I$^{1–93}$ fragment may contribute to the formation of a cross-β structure. The two β-strands face each other and are formed by residues 15–27 and 54–64 of the individual apoA-I$^{11–65}$ monomers, respectively. Successively stacked monomers along the fibril axis lead to the formation of two facing β-sheets running parallel towards the same axis, as in the apoC-II model (Fig. 5). Stacking of consecutive apoA-I monomers may be stabilized by the formation of intermolecular salt bonds, formed between K23 of the first β-strand of each monomer and E62 located at the second β-strand of the next molecule (Fig. 5). Apart from stabilizing this complex structure, the formation of these salt bonds may also compensate for the buried charges of residues K23

Table 1
Bands observed in the ATR FT-IR spectra produced from hydrated films of all the "aggregation-prone" peptides, after self-assembly, and their tentative assignments (Fig. 4).

Bands (cm^{-1})				Assignment
LATVYDVL	VTSTFS	VTQEFW	VSFLSA	
1138	1138	1138	1138	TFA
1186	1184	1184	1186	TFA
1204	1201	1203	1201	TFA
–	1496	1495	1496	Phe
1516	–	–	–	Tyr
1541	1528–1535	1535	1533	β-Sheet (amide II)
1626	1630	1631	1626	β-Sheet (amide I)
1668	1670	1666	1674	TFA
1693	1696	1697	1696	Antiparallel β-sheet

and E62, in a similar manner to the model proposed for apoC-II [33]. Interestingly, two of the "aggregation-prone" peptides proposed by our study, ^{14}LATVYVDVL^{22} and ^{53}VTSTFS^{58} correspond to major parts of the facing β-strands formed by each monomer of apoA-I (Fig. 5, shown in red and purple, respectively). Consequently, it seems possible that the high aggregation propensity and conformational properties of these two segments may promote polymerization of the "aggregation-prone" apoA-I$^{1–93}$ N-terminal fragment. Although this model provides some insight into how amyloid fibrils may be formed in familial apoA-I amyloidosis, it does not propose how amyloid fibrils are formed by the full length protein.

An alternative model was also recently proposed, based on FRET analysis, suggesting that the "aggregation-prone" 1–83 segment of apoA-I containing the point mutation G26R, forms amyloid protofibrils by folding in a relative β-strand–loop–β-strand arrangement [45]. The β-strands, which have an antiparallel direction in this case, are longer since they embrace 14–31 and 41–58 residues, respectively. However, similarly to our model, both the ^{14}LATVYVDVL^{22} and ^{53}VTSTFS^{58} peptides correspond to major parts of the facing β-strands. Additionally, as in our model, this β-hairpin is also proposed to be stabilized by the formation of a salt bridge, which is however formed by different residues, specifically between residues R26 and D48. Consequently, although the two models share both common characteristics and differences, the "aggregation-prone" ^{14}LATVYVDVL^{22} and ^{53}VTSTFS^{58} peptides apparently vitally contribute in the formation of apoA-I amyloid fibrils in both cases.

In conclusion, our work attempts to elucidate that the ^{14}LATVYVDVL^{22}, ^{53}VTSTFS^{58}, ^{67}VTQEFW^{72} and ^{227}VSFLSA^{232} peptides are core segments with chameleon properties which may lead both apoA-I$^{1–93}$ and full length apoA-I in the formation of amyloid deposits in familial amyloidosis and atherosclerosis, due to their intrinsic high propensity to self-aggregate. Furthermore, our computational studies indicate that the ^{14}LATVYVDVL^{22}, ^{53}VTSTFS^{58} peptides may also vitally contribute to the formation of amyloid fibrils associated with familial apoA-I amyloidosis. Targeted therapies focused on inhibiting the aggregation potency of the aforementioned segments may help to efficiently prevent or decelerate deposition of apoA-I species both in hereditary or aquired forms of apoA-I amyloidoses.

Conflict of interest

The authors declare that there are no conflicts of interest.

Acknowledgements

We should like to thank Dr. Evangelia Chrysina for help with the X-ray experiments and the Institute of Biology, Medicinal Chemistry and Biotechnology, National Hellenic Research Foundation for allowing us to use the X-ray protein crystallography facility. The help of Dr. George Baltatzis and Prof. Efstratios Patsouris and the use of the Morgagni Microscope at the 1st Department of Pathology, Medical School, University of Athens are also gratefully acknowledged. The authors sincerely thank the Editor in Chief and the Managing Editor for properly handling this manuscript and the anonymous reviewers for their very useful and constructive criticism, which helped us to improve the manuscript. We also thank the University of Athens for support.

Appendix A. Supplementary data

Supplementary data associated with this article can be found, in the online version, at http://dx.doi.org/10.1016/j.ijbiomac.2015.05.032

References

[1] M.N. Oda, R.O. Ryan, Apolipoprotein A-I structure, in: High-Density Lipoproteins, Wiley-VCH Verlag GmbH & Co. KGaA, 2008, pp. 1–23.
[2] D. Bashtovyy, M.K. Jones, G.M. Anantharamaiah, J.P. Segrest, J. Lipid Res. 52 (2011) 435–450.
[3] V.I. Zannis, S.K. Karathanasis, H.T. Keutmann, G. Goldberger, J.L. Breslow, Proc. Natl. Acad. Sci. U. S. A. 80 (1983) 2574–2578.
[4] R.T. Nolte, D. Atkinson, Biophys. J. 63 (1992) 1221–1239.
[5] J.P. Segrest, M.K. Jones, H. De Loof, C.G. Brouillette, Y.V. Venkatachalapathi, G.M. Anantharamaiah, J. Lipid Res. 33 (1992) 141–166.
[6] J.P. Segrest, D.W. Garber, C.G. Brouillette, S.C. Harvey, G.M. Anantharamaiah, Adv. Protein Chem. 45 (1994) 303–369.
[7] S. Lund-Katz, M.C. Phillips, Subcell. Biochem. 51 (2010) 183–227.
[8] M.G. Sorci-Thomas, S. Bhat, M.J. Thomas, Clin. Lipidol. 4 (2009) 113–124.
[9] J.F. Oram, J.W. Heinecke, Physiol. Rev. 85 (2005) 1343–1372.
[10] O. Gursky, X. Mei, D. Atkinson, Biochemistry 51 (2012) 10–18.
[11] S. Raimondi, F. Guglielmi, S. Giorgetti, S. Di Gaetano, A. Arciello, D.M. Monti, A. Relini, D. Nichino, S.M. Doglia, A. Natalello, P. Pucci, P. Mangione, L. Obici, G. Merlini, M. Stoppini, P. Robustelli, G.G. Tartaglia, M. Vendruscolo, C.M. Dobson, R. Piccoli, V. Bellotti, J. Mol. Biol. 407 (2011) 465–476.
[12] L. Obici, G. Franceschini, L. Calabresi, S. Giorgetti, M. Stoppini, G. Merlini, V. Bellotti, Amyloid 13 (2006) 191–205.
[13] A. Andreola, V. Bellotti, S. Giorgetti, P. Mangione, L. Obici, M. Stoppini, J. Torres, E. Monzani, G. Merlini, M. Sunde, J. Biol. Chem. 278 (2003) 2444–2451.
[14] P. Westermark, G. Mucchiano, T. Marthin, K.H. Johnson, K. Sletten, Am. J. Pathol. 147 (1995) 1186–1192.
[15] Y.Q. Wong, K.J. Binger, G.J. Howlett, M.D. Griffin, Proc. Natl. Acad. Sci. U. S. A. 107 (2009) 1977–1982.
[16] P.K. Teng, D. Eisenberg, Protein Eng. Des. Sel. 22 (2009) 531–536.
[17] M. Lopez de la Paz, L. Serrano, Proc. Natl. Acad. Sci. U. S. A. 101 (2004) 87–92.
[18] N.N. Louros, V.A. Iconomidou, P.L. Tsiolaki, E.D. Chrysina, G.E. Baltatzis, E.S. Patsouris, S.J. Hamodrakas, FEBS Lett. 588 (2013) 52–57.
[19] V.A. Iconomidou, A. Leontis, A. Hoenger, S.J. Hamodrakas, FEBS Lett. 587 (2013) 569–574.
[20] N.N. Louros, V.A. Iconomidou, P. Giannelou, S.J. Hamodrakas, PLOS ONE 8 (2013) e73258.
[21] N.N. Louros, N. Petronikolou, T. Karamanos, P. Cordopatis, V.A. Iconomidou, S.J. Hamodrakas, Biopolymers 102 (2014) 427–436.
[22] Y.Q. Wong, K.J. Binger, G.J. Howlett, M.D. Griffin, FEBS Lett. 586 (2012) 1754–1758.
[23] E. Adachi, A. Kosaka, K. Tsuji, C. Mizuguchi, H. Kawashima, A. Shigenaga, K. Nagao, K. Akaji, A. Otaka, H. Saito, FEBS Lett. 588 (2014) 389–394.
[24] M. Das, X. Mei, S. Jayaraman, D. Atkinson, O. Gursky, FEBS J. 281 (2014) 2525–2542.
[25] P. Mendoza-Espinosa, D. Montalvan-Sorrosa, V. Garcia-Gonzalez, A. Moreno, R. Castillo, J. Mas-Oliva, Mol. Cell. Biochem. 393 (2014) 99–109.
[26] A. Trovato, F. Seno, S.C. Tosatto, Protein Eng. Des. Sel. 20 (2007) 521–523.
[27] K.K. Frousios, V.A. Iconomidou, C.M. Karletidi, S.J. Hamodrakas, BMC Struct. Biol. 9 (2009) 44.
[28] A.C. Tsolis, N.C. Papandreou, V.A. Iconomidou, S.J. Hamodrakas, PLOS ONE 8 (2013) e54175.
[29] G. Romhanyi, Virchows Arch. A: Pathol. Anat. Histopathol. 354 (1971) 209–222.
[30] Oxford Diffraction, Oxford Diffraction Ltd., Abingdon, Oxfordshire, England, 2009.
[31] A.G.W. Leslie, H.R. Powell, Processing diffraction data with mosflm, in: R. Read, J.L. Sussman (Eds.), Evolving Methods for Macromolecular Crystallography, Springer, Dordrecht, The Netherlands, 2007, pp. 41–51.
[32] A. Savitsky, M.J.E. Golay, Anal. Chem. 36 (1964) 1627–1639.
[33] C.L. Teoh, C.L. Pham, N. Todorova, A. Hung, C.N. Lincoln, E. Lees, Y.H. Lam, K.J. Binger, N.H. Thomson, S.E. Radford, T.A. Smith, S.A. Muller, A. Engel, M.D. Griffin, I. Yarovsky, P.R. Gooley, G.J. Howlett, J. Mol. Biol. 405 (2010) 1246–1266.
[34] C.C. Luo, W.H. Li, M.N. Moore, L. Chan, J. Mol. Biol. 187 (1986) 325–340.
[35] W.H. Li, M. Tanimura, C.C. Luo, S. Datta, L. Chan, J. Lipid Res. 29 (1988) 245–271.
[36] R. Apweiler, A. Bairoch, C.H. Wu, W.C. Barker, B. Boeckmann, S. Ferro, E. Gasteiger, H. Huang, R. Lopez, M. Magrane, M.J. Martin, D.A. Natale, C. O'Donovan, N. Redaschi, L.S. Yeh, Nucleic Acids Res. 32 (2004) D115–D119.
[37] J.D. Thompson, D.G. Higgins, T.J. Gibson, Nucleic Acids Res. 22 (1994) 4673–4680.
[38] N. Eswar, B. Webb, M.A. Marti-Renom, M.S. Madhusudhan, D. Eramian, M.Y. Shen, U. Pieper, A. Sali, Curr. Protoc. Bioinform. 5 (2006), Unit 5.6.
[39] K. Hinsen, J. Comput. Chem. 21 (2000) 79–85.
[40] E.F. Pettersen, T.D. Goddard, C.C. Huang, G.S. Couch, D.M. Greenblatt, E.C. Meng, T.E. Ferrin, J. Comput. Chem. 25 (2004) 1605–1612.
[41] G. Vriend, J. Mol. Graph. 8 (1990) 52–56, 29.
[42] P. Sevugan Chetty, L. Mayne, Z.Y. Kan, S. Lund-Katz, S.W. Englander, M.C. Phillips, Proc. Natl. Acad. Sci. U. S. A. 109 (2012) 11687–11692.
[43] S.J. Hamodrakas, Comput. Appl. Biosci. 4 (1988) 473–477.

[44] C. Kim, J. Choi, S.J. Lee, W.J. Welsh, S. Yoon, Nucleic Acids Res. 37 (2009) W469–W473.
[45] M. Girych, G. Gorbenko, V. Trusova, E. Adachi, C. Mizuguchi, K. Nagao, H. Kawashima, K. Akaji, S. Lund-Katz, M.C. Phillips, H. Saito, J. Struct. Biol. 185 (2014) 116–124.
[46] X. Mei, D. Atkinson, J. Biol. Chem. 286 (2011) 38570–38582.
[47] D.W. Borhani, D.P. Rogers, J.A. Engler, C.G. Brouillette, Proc. Natl. Acad. Sci. U. S. A. 94 (1997) 12291–12296.
[48] J.P. Segrest, M.K. Jones, B. Shao, J.W. Heinecke, Biochemistry 53 (2014) 7625–7640.